THE JOURNAL OF PHYSICAL CHEMISTRY B
A JOURNAL OF THE AMERICAN CHEMICAL SOCIETY

pubs.acs.org/JPCB

Article

Nanoconfinement Raises the Energy Barrier to Hydrogen Atom Exchange between Water and Glucose

Published as part of The Journal of Physical Chemistry virtual special issue "Dor Ben-Amotz Festschrift".

Samantha L. Miller, Benjamin P. Wiebenga-Sanford, Christopher D. Rithner, and Nancy E. Levinger*

Cite This: *J. Phys. Chem. B* 2021, 125, 3364–3373

Read Online

ACCESS | Metrics & More | Article Recommendations | Supporting Information

ABSTRACT: In bulk aqueous environments, the exchange of protons between labile hydroxyl groups typically occurs easily and quickly. Nanoconfinement can dramatically change this normally facile process. Through exchange spectroscopy (EXSY) NMR measurements, we observe that nanoconfinement of glucose and water within AOT (sodium bis(2-ethylhexyl) sulfosuccinate) reverse micelles raises the energy barrier to labile hydrogen exchange, which suggests a disruption of the hydrogen bond network. Near room temperature, we measure barriers high enough to slow the process by as much as 2 orders of magnitude. Although exchange rates slow with decreasing temperatures in these nanoconfined environments, the barrier we measure below ~285 K is 3−5 times lower than the barrier measured at room temperature, indicating a change in mechanism for the process. These findings suggest the possibility of hydrogen tunneling at a surprisingly high-temperature threshold. Furthermore, differences in exchange rates depend on the hydroxyl group position on the glucose pyranose ring and suggest a net orientation of glucose at the reverse micelle interface.

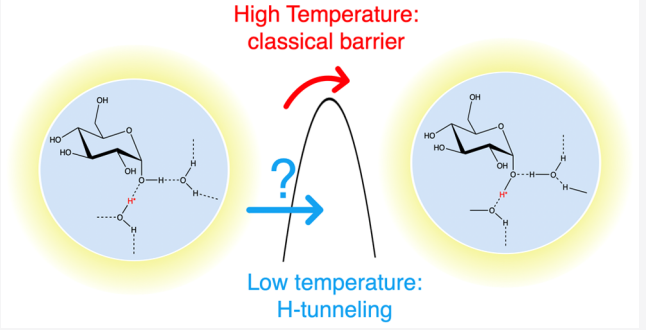

INTRODUCTION

Water is a ubiquitous molecule integral to numerous fields such as chemistry, engineering, biology, environmental studies, and medicine. Knowledge of water's structure, dynamics, kinetics, and phase transition behavior has been well described, especially in the bulk liquid phase.[1,2] Because of its importance, researchers have rigorously studied this molecule and defined many of its unique bulk phase properties such as its high heat capacity and surface tension, volumetric expansion upon transition from liquid to solid phase, and maximum density at 277 K at atmospheric pressure. Water's strong hydrogen bonding ability leads to many of these unique characteristics. Through hydrogen bonding, protons on water can easily transfer onto or from other molecules.[3,4] In bulk aqueous solution, proton exchange from water to other hydrogen bonding moieties, such as alcohols, amines, or amides, is generally extremely facile.[5−7] The ease of proton exchange in aqueous solutions has wide-ranging effects, such as the Grotthuss mechanism, in which protons diffuse through water at rates substantially faster than other ions.[8]

When restricted to nanosized spaces, water demonstrates properties and dynamics that differ from its bulk phase behavior.[9−11] Researchers across numerous fields have achieved confinement in a myriad of ways: within carbon or lipid nanotubes,[12−14] in suspended aerosols,[15,16] in silica pores,[17,18] and solvated in reverse micelles,[19,20] the method we use in this study. Confinement in reverse micelles results in a departure from bulk aqueous behavior, as exemplified in early studies by Radhakrishnan et al. that demonstrated confinement to nanosized pores stabilized the hexagonal water phase over a large range of temperatures,[21] where smaller pores led to a more dramatic freezing point depression.

Reverse micelles provide a relatively stable and size tunable nanoenvironment for studying the effects of confinement.[22,23] After physical perturbation, the ternary mixture of polar (usually aqueous), nonpolar, and amphiphilic components self-assemble into droplets wherein the polar heads of the amphiphilic surfactant face inward around the polar droplet. A number of characteristics make reverse micelles ideal as a model system for investigating confined spaces, including their thermodynamic stability over long periods, spontaneous formation, and transparent appearance. The unitless parameter w_0 describes the approximate size of the reverse micelle:

Received: November 28, 2020
Revised: February 19, 2021
Published: March 30, 2021

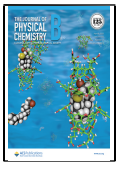

https://doi.org/10.1021/acs.jpcb.0c10681
J. Phys. Chem. B 2021, 125, 3364–3373

$$w_0 = \frac{[\text{water}]}{[\text{surfactant}]} \quad (1)$$

Additionally, the viscosity of reverse micelle solutions is comparable to that of the pure nonpolar organic solvent facilitating a range of experiments, for example, NMR spectroscopy.[24] When prepared with the surfactant aerosol OT (AOT), the reverse micelle headgroup comprises the negatively charged sulfonate group accompanied by the positively charged sodium counterion. Inexpensive and nontoxic, AOT is the most widely used surfactant when preparing reverse micelles and is the amphiphile used in this study. Characterization by small-angle X-ray scattering, small-angle neutron scattering, and dynamic light scattering has given scientists a good understanding of AOT reverse micelles.[25,26] The encapsulated water molecules that form the core of the reverse micelle can interact with other molecules dissolved in the reverse micelle, for example, osmolytes, proteins, and probe molecules.[27−31]

We have previously reported how nanoscale confinement in reverse micelles dramatically slows the exchange behavior of water hydrogen atoms to the hydroxyl groups on glucose, as observed qualitatively using 1D ^{1}H NMR and quantified using exchange spectroscopy (EXSY) NMR techniques.[28] This slowed exchange demonstrates that confinement has significant effects on chemical processes beyond restriction of molecular translation. The mechanisms of exchange and network disruption occurring in our simplified reverse micelle model may be present in the more complicated biological systems, especially those involving glucose regulated proteins and glycan signaling.[32,33] Hydrogen atom exchange between water and glucose in reverse micelles provides a model to increase understanding of a wide variety of biological processes that involve nanoscale environments.[28] In the work reported here, we use the same EXSY NMR technique to directly measure exchange rate constants as a function of temperature, calculate the activation energy barrier to hydrogen atom exchange between water and glucose, and discuss possible effects that confinement has on the mechanism responsible for that process.

MATERIALS AND METHODS

D-(+)-Glucose (99.9%), aerosol OT (AOT, (bis(2-ethylhexyl) sulfosuccinate sodium salt, 99.9%), 2,2,4-trimethylpentane (isooctane, 99.9%), and cyclohexane-d_{12} (99.9%) were purchased from MilliporeSigma (Burlington, MA) and used as received. D_2O was acquired from Cambridge Isotope Laboratories. For brevity, "glucose" is used to refer to D-(+)-glucose and "isooctane" to refer to 2,2,4-trimethylpentane throughout. When appropriate, a particular anomer of glucose is specified. Water was Millipore filtered for 18 MΩ·cm resistivity. All glassware used was rigorously cleaned, acid washed with concentrated HNO_3, rinsed with Millipore filtered water, and thoroughly dried.

Reverse micelles were prepared from 0.1 M AOT stock solutions in isooctane. Solid AOT was added gravimetrically to isooctane to achieve a 0.1 M concentration. Next, water was added to form the reverse micelle nanodroplets. All reverse micelles reported here were prepared to w_0 = 10. The reverse micelle solution was sonicated for 45 min, glucose was loaded to achieve a 1:30 glucose:water mole ratio, and further sonicated for 30 min until no solid glucose was detected. The overall glucose concentration in the reverse micelles suspended in isooctane was 30 mM. Within the water core of the reverse micelles, the glucose concentration was ∼1.8 M.

For ^{2}H NMR experiments, hydroxyl groups on glucose were exchanged for OD by dissolution of glucose in D_2O and subsequent evaporation to dryness in a desiccator. Reverse micelle samples were prepared in the same fashion as described for protonated samples but using D_2O and deuterium-exchanged glucose.

NMR spectra, both ^{1}H and 1D EXSY, were collected by using a 500 MHz spectrometer (Agilent Inova) operating at 11.75 T. In preparation for NMR spectra collection, reverse micelle mixtures were mixed with a cyclohexane-d_{12} lock solvent (2 vol %). Spectra were collected at nine temperatures: 304, 298, 288, 283, 273, 268, 264, 258, and 252 K (31, 25, 15, 10, 0, −5, −9, −15, and −21 °C). Temperature settings on the Varian NMR temperature controller were confirmed via methanol thermometer calibration (Figure S1).[34] To ensure thermal stability of the NMR probe, thus the sample throughout the measurement, we equilibrated samples in the NMR for 30 min before experiments were performed to ensure thermal stability of the NMR probe and sample.

Each experiment began with collection of a 1D ^{1}H NMR spectrum. Next, the 1D EXSY NMR spectra were collected. We use a NOESY-based EXSY method[28] whose pulse scheme exploits the effects of magnetization transfer, when one spin generates a local magnetic field that subsequently perturbs the spin on a nearby atom.[35−37] As a standard feature in the Agilent software package, Vnmrj version 4.2, this EXSY pulse scheme uses the principles of saturation transfer to track the physical exchange of excited water hydrogens onto glucose hydroxyls. Pulse widths were set for each experiment to ensure water protons underwent a precise 90° spin flip into the observable xy plane. The hard $\pi/2$ pulse was 5.6 μs. The 1D EXSY mixing times (in seconds) were assigned to the following values: 0.0, 0.002, 0.01, 0.05, 0.07, 0.1, 0.2, 0.4, 0.6, 0.8, 1.0, 1.5, 2.0, and 2.5. Because the exchange signal completely decayed after 2.5 s, mixing times did not exceed this value. The hard pulse excited hydrogen atoms on water molecules that subsequently exchange onto glucose during the mixing period; this results in the appearance of the glucose hydroxyl peaks. The mixing period, or exchange delay, follows the selective π-pulse that labels a frequency-defined spin across its full width half-height frequency. The integrated intensity of the glucose OH peaks allows us to quantify the exchange rates as they are a direct result of the hydrogen's transition from water to glucose. We repeated this 1D EXSY experiment for each temperature measured. Lowering the temperature changed the chemical shift of the water peak, requiring experimental adjustments to acquire reliable spectra at each temperature.

All NMR spectra were processed in MNOVA (ver. 12.0.4-22023). The size of the direct FID was 32768 data points. All spectra were processed by using zero-filling with twice the number of data points and apodization with a 1.00 Hz exponential weighting function. Individual spectral peaks were fitted with Lorentzian−Gaussian line shapes by using MNOVA software and subsequently integrated.

To ensure that samples remained fully emulsified reverse micelles over the entire temperature range examined, we measured our samples with changing temperature using several different methods. First, we observed samples visually over the range of temperatures used for NMR measurements. Over the entire temperature range probed, 252 to 304 K (−21 to 31 °C), we observed clear, nonviscous solutions with no evidence

https://doi.org/10.1021/acs.jpcb.0c10681
J. Phys. Chem. B 2021, 125, 3364−3373

of ice formation on NMR tube walls or at the bottom. We also measured the viscosity of each reverse micelle sample using a Cannon-Fenske 9721-B74 (Cole Parmer) viscometer as a function of temperature. The setup included a temperature-controlled water bath accurate to 0.1 K as well as an electronic timer for measuring efflux through the glass tube. Each viscosity measurement was repeated in triplicate. Reverse micelle formation and sizes were measured as a function of temperature via dynamic light scattering measurements (DLS, Malvern Zetasizer Nano ZS) in backscatter mode (173°). Measurements were performed in triplicate to extract average size which we report based on the number distribution. Reverse micelle sizes were measured as a function of temperature to the lowest limit afforded by the instrument (275 K, see the Supporting Information). Two-minute equilibration between measurements provided stable uniform temperature distribution in samples. Finally, we measured reverse micelle solutions via differential scanning calorimetry (DSC2500, TA Instruments). Glucose-loaded reverse micelle mixtures were placed into Tzero hermetic aluminum pans (TA Instruments) and fully sealed prior to collection; sample mass did not exceed 50.00 mg. Temperature sweeps (10 °C/min) were performed over the range 238−303 K, matching the range of temperatures probed in the 1D EXSY NMR experiments. Each of these experiments, as well as NMR studies, demonstrated reversible behavior for samples that did not require additional agitation to restore reverse micelle formation.

RESULTS

The goal of the study reported here is to determine the activation energy barrier to hydrogen atom exchange between water and glucose that arises from confinement in reverse micelles. In aqueous solution and in reverse micelles, glucose exists as both the α-D-glucose and β-D-glucose anomer (Figure 1). We use 1D EXSY NMR, sometimes called the zz-exchange

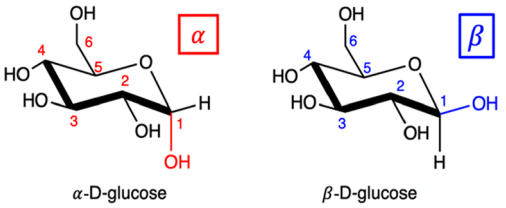

Figure 1. Chemical structures for the pyranose form of the two glucose anomers present in solution. Numbers refer to both the carbon and hydroxyl group; e.g., hydroxyl group 2 is attached to carbon 2. Carbon 1 is the anomeric carbon, with the colored hydroxyl groups indicating the difference between α (red) and β (blue) glucose anomers.

experiment,[38] to measure the physical migration of a hydrogen atom from water to glucose, as given in eq 2

$$\mathrm{HOH^{*}} + \mathrm{GOH} \underset{k_{-1}}{\overset{k_1}{\rightleftharpoons}} \mathrm{HOH} + \mathrm{GOH^{*}} \overset{k_2}{\rightarrow} \mathrm{HOH} + \mathrm{GOH} \tag{2}$$

where HOH represents water, GOH represents a glucose hydroxyl, and HOH* indicates a water molecule whose hydrogen has been energetically labeled with a radio-frequency pulse. The rate constant k_1 quantifies the rate of hydrogen exchange from water to glucose while k_{-1} indicates the reverse process. We assume that $k_1 \gg k_{-1}$ due to the high pK_a of glucose (p$K_a \approx 12$).[28] The rate constant k_2 indicates spin−lattice relaxation back to equilibrium.

To measure the barrier to exchange, we determine the temperature-dependent exchange rate so that we can construct an Arrhenius plot. For each temperature point, we collect a series of EXSY NMR spectra as a function of mixing time. Figure 2 shows representative EXSY spectra acquired at a 100 ms mixing time at two different temperature points, 298 and 252 K.

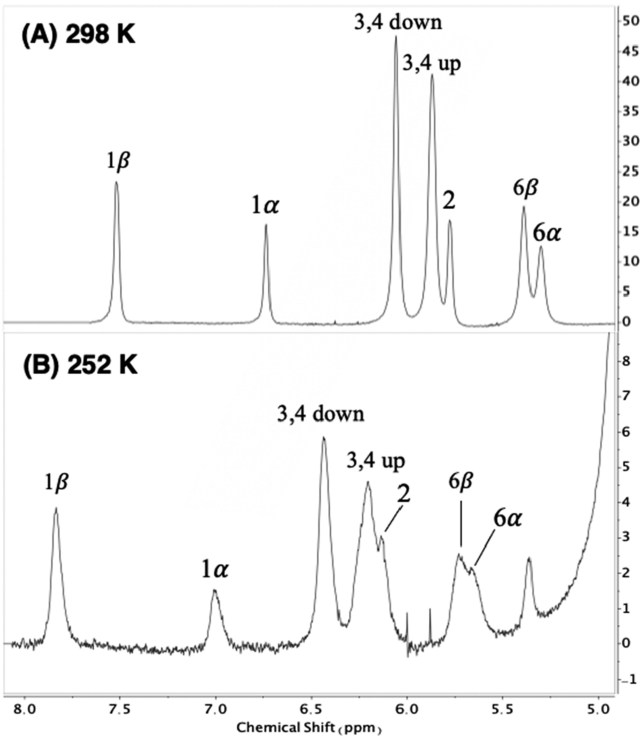

Figure 2. 1D EXSY NMR spectra for 1:30 glucose:water in 0.1 M AOT in isooctane collected at (A) 298 K and (B) 252 K. Each spectrum represents the system at the same 100.0 ms mixing time. Peaks associated with hydroxyls at carbons 3 and 4 cannot be distinguished, thus labeled 3,4 up and 3,4 down indicating upfield/downfield shifts.

The following figures follow the order of peak appearance in the NMR spectra. The signal-to-noise ratio decreases with decreasing temperature as peak intensity drops and peaks broaden. The spectral peaks associated with 1α and 1β hydroxyl groups at the anomeric carbon appear furthest downfield and are well separated from other signals. This makes them the most straightforward and reliable to analyze; thus, we focus on these signals for the full temperature range. Trends observed from the 1α and 1β hydroxyl signals are also observed for the other hydroxyl signals. The area under individual spectral peaks reflects the population of spin excited protons exchanged from water onto glucose at the mixing time the spectrum was collected in the EXSY experiment as represented by k_1 in eq 2.[28]

We observe a downfield chemical shift of the water and glucose hydroxyl group signals as a function of decreasing temperature as shown in Figure 3. Shifts for signals arising from all hydroxyl groups follow similar trends and display a linear dependence on temperature.

https://doi.org/10.1021/acs.jpcb.0c10681
J. Phys. Chem. B 2021, 125, 3364−3373

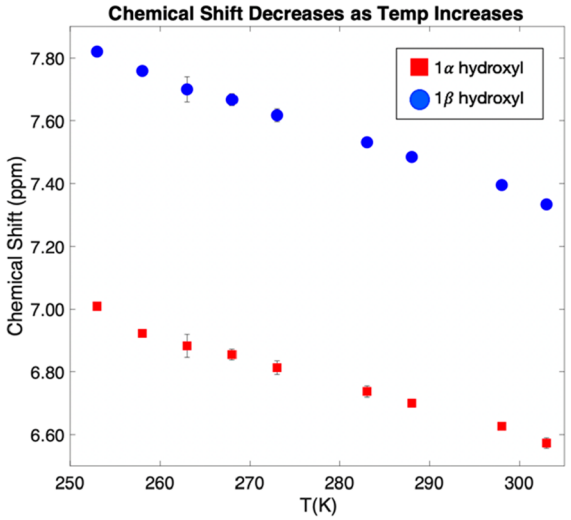

Figure 3. Chemical shift as a function of temperature for peaks corresponding to the glucose anomeric 1α and 1β hydroxyl groups. Error bars represent the standard deviation between three replicate measurements of the same sample.

We determined the water to glucose hydrogen exchange rates at each temperature from plots of integrated intensity as a function of mixing time. These data were fitted to eq 3

$$[\mathrm{GOH}^*] = \frac{k_1}{k_2 - k_1}[\mathrm{GOH}]_0(\mathrm{e}^{-k_1 t} - \mathrm{e}^{-k_2 t})\mathrm{e}^{-t/T_1} + C \tag{3}$$

which describes the chemical process given in eq 2; the exponential decay with time T_1 reflects the spin−lattice relaxation of water that can occur before the chemical exchange process begins. Using custom code written in Matlab, we extract the desired k_1 and k_2 rate constants (Table S1). To account for the temperature dependence of the intramicellar water T_1, we use the slope of the temperature-dependent values for bulk water measured by Tsukiashi et al. to extrapolate using published values for bulk water T_1 and T_1 in AOT reverse micelles measured by Kassab.[39] Including T_1 in the kinetic analysis reduces the values for both k_1 and k_2. To confirm the validity of this extrapolation, we observe that either over- or underestimation of the T_1 value by 10% leaves the resulting rate constants within the original margin of error calculated for replicate measurements. As $k_1 \gg k_{-1}$, we omit the reverse process in the eq 3 integrated rate law. Figure 4 displays the integrated intensity for exchange from water to the 1α hydroxyl group of the α-D-glucose anomer as mixing time increases for spectra collected at 298 and 252 K along with curves fitted to eq 3. Initially, integrated intensity increases as hydrogen atom exchange begins. The integrated intensity decreases as spin decays out of the system toward equilibrium. At 298 K, k_1 is larger than it is at 252 K as indicated by the steeper initial slope. Conversely, k_2 is larger at 252 K than at 298 K. Signals for data at other temperatures and for other hydroxyl groups appear similar.

In addition to analyzing the exchange process for the 1α and 1β anomeric hydroxyls, we also explored the rate of hydrogen atom exchange with the four other glucose hydroxyl groups at carbons 2, 3, 4, and 6 (see Figure 1). Because the NMR signals for the anomeric hydroxyl groups are well separated from other hydrogens, we can quantitatively evaluate their integrated intensities across the entire temperature range measured. At

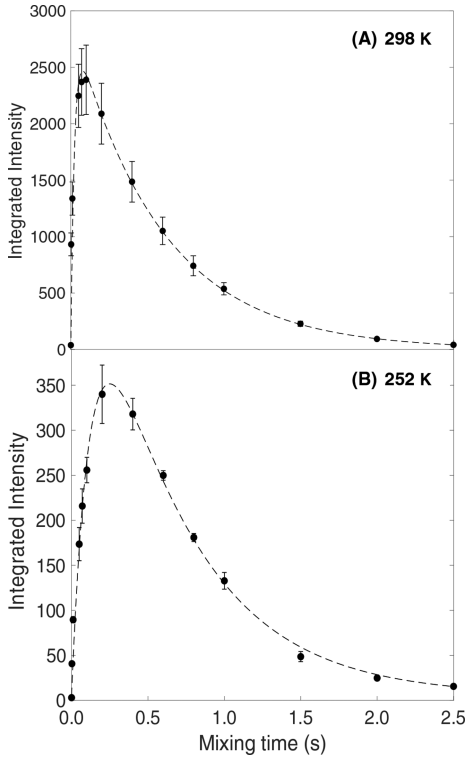

Figure 4. Integrated intensity of NMR peaks from EXSY experiments as a function of mixing time for the glucose 1α hydroxyl in w_0 = 10 AOT reverse micelles at (A) 298 K (25 °C) and (B) 252 K (−21 °C). Error bars reflect the standard deviation between three replicate measurements of the same sample.

temperatures higher than 273 K, all the glucose hydroxyl peaks are sufficiently well-separated to determine exchange rates and rate constants k_1 and k_2. Figure 5 shows the exchange rate constants as a function of decreasing temperature in this high-temperature regime. However, as the temperature drops, the

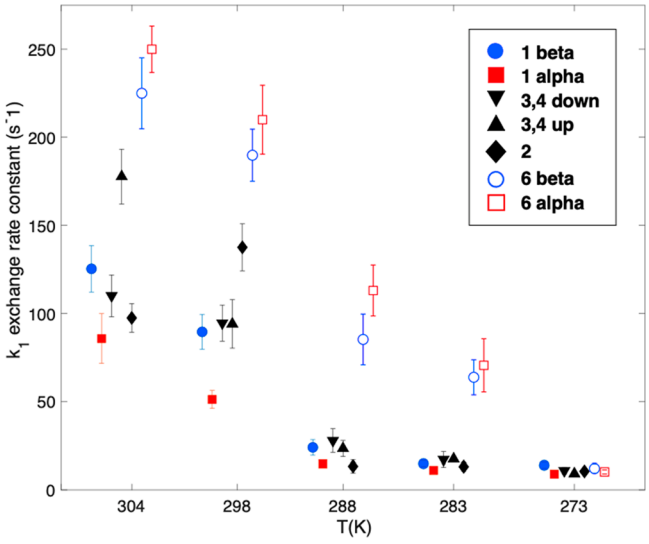

Figure 5. Rate constants for hydrogen atom exchange between water and glucose hydroxyl at each carbon position on the glucose ring as a function of decreasing temperature. Rate constants were measured for each hydroxyl at each labeled temperature, but data points in each cluster are offset on the x-axis for clarity. Error bars reflect uncertainty propagated from three replicate measurements of the same sample.

https://doi.org/10.1021/acs.jpcb.0c10681
J. Phys. Chem. B 2021, 125, 3364−3373

signals associated with hydroxyl groups on carbons 2, 3, 4, and 6 broaden and merge, as shown in Figure 2. This prohibits quantitative integrations to yield accurate rates. Table S1 reports values for k_1 and k_2 extracted from the fitted curves for all temperatures investigated.

We observe that the k_1 rate constants decrease with decreasing temperature as less thermal energy is available to the system to overcome the barrier to physical exchange. As the solution cools, the overall viscosity of the reverse micelle solution increases, leading to longer correlation times, as expected. The increase in k_2 combined with broadening of the water peak with decreasing temperature suggests the intramicellar water becomes more viscous with decreasing temperatures, resulting in longer correlation times, shorter T_1 times, and thus higher relaxation rates; although we do not measure the T_1 lifetime or viscosity directly, broadening of the water peak with decreasing temperature suggests the intramicellar water also becomes more viscous with decreasing temperatures. These longer correlation times result in shorter T_1 times and thus higher relaxation rates. This faster relaxation at lower temperatures agrees with expected trends for longer correlation times for water.[39,40] The approximately 2-fold change in the k_2 relaxation rate constant over the temperature range we explored is substantially smaller than the >20-fold change in the exchange constant, k_1, when transitioning from the highest to lowest temperature.

To determine an activation energy for chemical exchange between water and glucose, we constructed Arrhenius plots using the rate constants obtained at each temperature. Arrhenius plots characterizing the temperature-dependent hydrogen atom exchange for the 1α (Figure 6A) and 1α (Figure 6B) hydroxyl groups on glucose in the reverse micelle are presented. Each point represents the average k_1 rate extracted from three individual EXSY NMR experiments of the same sample at the chosen temperature; error bars indicate the standard deviation between measurements. Fits shown in Figure 6 reveal that a single linear fit does not accurately describe the data over the full temperature range measured, and the data are much better represented with separate linear fits to data in high- and low-temperature ranges, thus implying a change in exchange mechanism between high and low temperatures. Systematic divergence of the data from the single line fit, as well as the R^2 values, shows that fitting the data to high- and low-temperature ranges is superior to a single linear fit (Table S2).

Using the Arrhenius equation

$$\ln k = \ln A - \frac{E_A}{RT} \tag{4}$$

we obtain the activation energy, E_A, from the slopes of the fits. At temperatures above 285 K, we find the activation energies for exchange between water and glucose α and β anomers are 73.3 ± 6.1 and 76.8 ± 6.6 kJ/mol, respectively. Below the 285 K threshold, the activation energies drop to 11.8 ± 2.7 and 31.5 ± 6.9 kJ/mol for 1α and 1β hydroxyl groups, respectively.

We considered whether a phase transition in the reverse micelle solution could account for the observed change in slope and activation energy at low temperatures. With a freezing point of 166 K (−107.4 °C),[41] well below the temperatures explored during the EXSY NMR experiments, we do not expect or observe macroscopic freezing of the isooctane continuous phase, confirmed by differential scanning calorimetry experiments (Figure S2). However, the complex

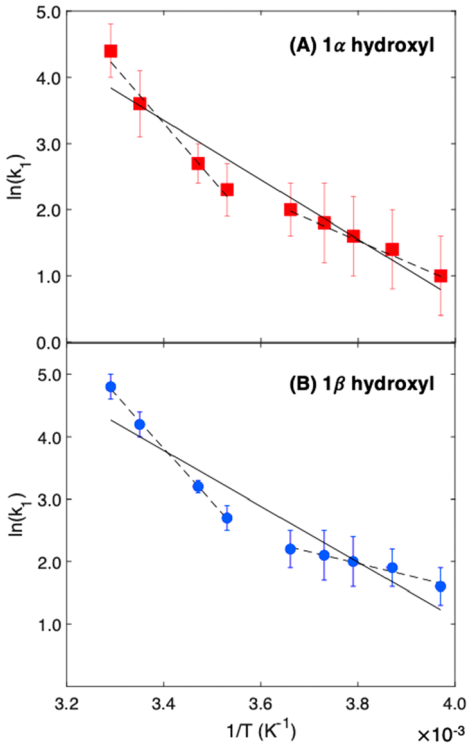

Figure 6. Arrhenius plots of hydrogen atom exchange rate as a function of inverse temperature and fits to single linear fit (solid lines) and linear fits to high- and low-temperature regimes (dashed lines): (A) 1α hydroxyl and (B) 1β hydroxyl. Error bars represent the standard deviation uncertainty from three measurements of the same sample.

quaternary reverse micelle solution could undergo a morphological phase transition, such as percolation from individual reverse micelles to a hexagonal inverted phase or sponge phase with decreasing temperature.[42,43] To assess such phase change, we performed dynamic light scattering (DLS) and viscosity measurements of the solutions as a function of temperature. DLS measurements indicated that solutions prepared with w_0 = 10 glucose loaded reverse micelles maintained individual nanosized particles although particles grew slightly larger and more polydisperse with decreasing temperature (Figure S4 and Table S3). Bulk viscosity increased smoothly with decreasing temperature, showing no significant jump that would be associated with a morphology change.[44] These measurements indicate that the source of the different activation energy measured at low temperatures does not arise from a vastly different microemulsion or physical (e.g., solid) phase.

DISCUSSION

In bulk aqueous solution, the hydrogen atom exchange between water and glucose can occur through two main mechanisms, either an acid- or a base-catalyzed charge transfer mechanism or through a concerted exchange mechanism in which two water molecules that are part of the larger water network act in concert to donate a proton from one water while the second simultaneously accepts a proton from glucose. In bulk water solutions at low or high pH (≤3 or ≥9), exchange rates are very fast, in excess of 10000 s^{-1}, but even near neutral pH, bulk water exchange occurs rapidly enough to result in the complete coalescence of glucose hydroxyl and water signals through exchange broadening in a

https://doi.org/10.1021/acs.jpcb.0c10681
J. Phys. Chem. B 2021, 125, 3364−3373

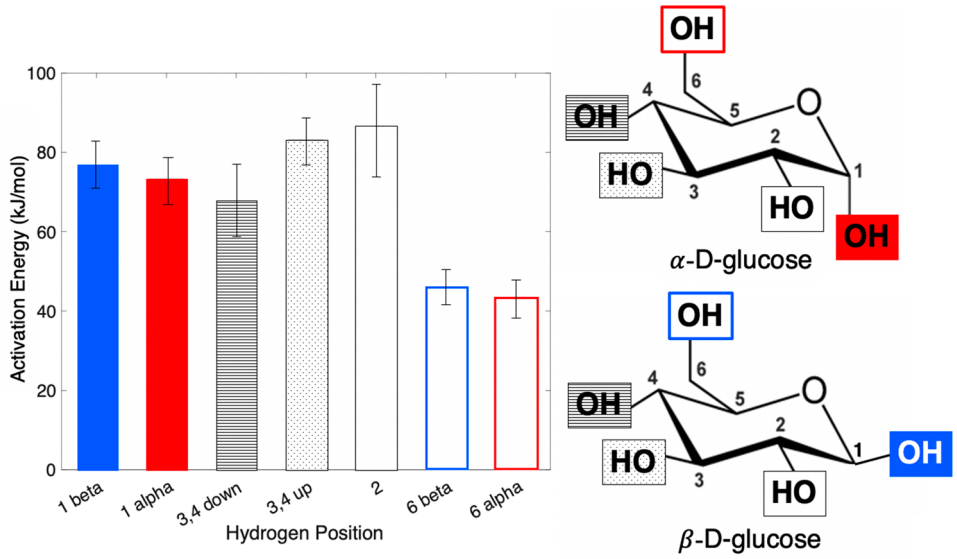

Figure 7. Activation energies for hydrogen atom exchange between water and glucose hydroxyl at each position on the glucose ring at temperatures above 285 K in kJ/mol. Structures of both anomers are provided to emphasize the differences relative to orientation in space.

typical 1D ^{1}H NMR experiment.[45] In a reverse micelle environment at or near neutral pH, exchange is slowed and individual glucose hydroxyl signals are observable, as we have previously reported.[28] Here we report the activation energy barrier to hydrogen exchange in an aqueous environment and find two separate temperature regimes indicated by two distinct linear regions in the Arrhenius plot about the temperature threshold of approximately 285 K (12 °C), estimated from the intersection of the linear fits to the two temperature regimes. The presence of two distinct temperature regimes for hydrogen atom exchange suggests two different primary exchange mechanisms for aqueous hydrogen exchange: one with a relatively high activation energy above 285 K and an activation energy almost 3 times lower at low temperature.

High-Temperature Regime. Our EXSY NMR spectral data have a high signal-to-noise ratio and yield high precision in the high-temperature regime, which degrades as temperature decreases. In this high-temperature regime, the measured activation energies for 1α and 1β hydroxyls are the same, within the calculated uncertainty. The good signal-to-noise achieved at higher temperatures allows us to analyze the exchange rate behavior of all glucose hydroxyl groups (Figure 5) and thus determine the activation energy for hydrogen atom exchange at each hydroxyl position on the glucose molecule, as shown in Figure 7. All the exchange rates decrease with decreasing temperature.

The exchange of water hydrogen atoms to glucose molecules nanoconfined in reverse micelles happens much more slowly than the process occurs in bulk water, making it possible for us to measure the activation energy associated with chemical exchange.[45−47] Several explanations can account for how confinement affects each exchange participant, that is, glucose and water. The confinement presented by the reverse micelle structure can disrupt the water hydrogen bond network that normally facilitates the concerted exchange between water molecules and glucose hydroxyl groups.[48] Rather than forming an extended, inextricably linked network of water molecules constantly breaking and re-forming hydrogen bonds, water must compete with the smothering presence of glucose and the AOT headgroups to complete the concerted exchange. In addition, water and/or glucose interactions with ions could disrupt the exchange process. For example, molecular dynamics simulations performed by Zhang et al. show how increased ion concentration slows the ability of water molecules to reorient and form new hydrogen bonds.[49] Crowding and direct interactions with ions present at the water−AOT interface may contribute to the energy barrier we measure here. We also considered the possibility of glucose stacking within the reverse micelles. Although glucose−glucose aggregation could block water from accessing glucose hydroxyl groups, reducing exchange rates, previous 2D NOESY NMR measurements showed no close interactions between glucose molecules that would support the existence of glucose aggregation.[27]

To interpret trends in the hydrogen atom exchange rates between glucose positions (scatter plot shown in Figure 5) and their associated activation energies, we consider two data cohorts: the 6α and 6β hydroxyl groups and all other hydroxyl groups. The first cohort, i.e., 6α and 6β hydroxyl groups, demonstrates consistently higher exchange rates than the latter cohort. At some temperatures, the difference is greater than a 2-fold increase. At 304 and 298 K, the latter cohort displays a broad distribution of exchange rates that collapse into one general rate at lower temperatures, within the error of the measurements. Within this second cohort, we observe no systematic trend except that the 1α hydroxyl exchange rate remains consistently smaller relative to the others. Even this rate eventually falls within the average exchange rate by 283 K.

The higher exchange rate for the 6α and 6β hydroxyl position also correlates to the lowest barrier for exchange of all the hydroxyl positions on the glucose molecule (Figure 7). This could indicate a net orientation of the glucose molecule such that the "free arm" associated with the 6α and 6β hydroxyl groups of the glucose pyranose form protrudes inward toward the reverse micelle water core. In this orientation, the 6α or 6β hydroxyl group could preferentially sample more bulklike water, facilitating its exchange with water's hydrogens. Interestingly, changing the anomeric hydroxyl group from 1α to 1β is sufficient to increase the

https://doi.org/10.1021/acs.jpcb.0c10681
J. Phys. Chem. B 2021, 125, 3364−3373

probability of exchange, as the exchange rate for the 1α anomeric hydroxyl group is consistently smaller than the 1β anomer, although within our ability to measure it the activation energy for hydrogen exchange does not differ between these two positions. Figure 7 displays all activation energies as a function of position on the glucose ring and reinforces the division into the same aforementioned cohorts based on activation energy. The cohort comprising the 6α and 6α hydroxyl position has a significantly smaller barrier to hydrogen atom exchange, with an average of 44.5 kJ/mol, compared to the second cohort comprising the rest of the hydroxyl positions, which has an average exchange barrier of 77.5 kJ/mol. We attribute this 74% increase to the steric hindrance posed by hydroxyl groups that likely reside close to the surfactant/water interface and therefore cannot exchange as easily as the 6α and 6β hydroxyl position.

Low-Temperature Regime. The reduced signal-to-noise and broadening of the signals in the low-temperature regime (below 285 K) cause poor spectral separation and preclude quantitative integration for all but the anomeric hydroxyls. The spectrum shown in Figure 2B is representative of the broadening and merged features typical of these overlapping hydroxyl signals. Thus, we limit our low-temperature analysis to the α and β anomeric hydroxyl groups. Considering the trends observed in the high-temperature regime, we expect the other hydroxyl groups demonstrate trends similar to the anomeric groups in the low-temperature regime.

As the reverse micelles cool, the exchange rate decreases. However, our differential scanning calorimetry results indicate that the decreased rate is not the result of a freezing event. Despite slower exchange rates than those in the high-temperature regime, the Arrhenius plots in the low-temperature regime display a significantly shallower slope associated with a lower activation energy. This difference suggests a different mechanism is responsible for the observed exchange process. We hypothesize that rather than overcoming the barrier to exchange, hydrogen atoms tunnel from water to glucose. Reports of hydrogen atom tunneling in related systems such as nanowater clusters and monolayered water molecules.[50,51] show that nuclear quantum effects extend the hydrogen−oxygen bond, thereby delocalizing the hydrogens and leaving them susceptible to participate in hydrogen bonds with surrounding molecules.[52] Additionally, reports in the literature suggest that hydrogen bonds get stronger as temperature drops,[53] which can increase the probability of hydrogen tunneling and facilitate hydrogen atom exchange. The increasing chemical shift we observe with decreasing temperature (Figure 3) indicates strengthening hydrogen bonding with lower temperature. Furthermore, the confined space created by the reverse micelle could facilitate hydrogen bond shortening, which is regarded as essential to initiate proton tunneling.[54]

To probe the possibility of a hydrogen atom tunneling mechanism, we attempted to test our hypothesis in ^{2}H EXSY NMR experiments replacing H_2O with D_2O, deuterating glucose molecules, and following the OD signature with ^{2}H NMR. By substituting D_2O for H_2O, we expect the heavier ^{2}H isotope to suppress hydrogen tunneling and yield rate constants consistent with the steeper trend in the high-temperature regime. We deuterated the hydroxyl hydrogens on glucose and prepared reverse micelles with D_2O. However, unlike the case with H_2O and protonated glucose, confinement of deuterated glucose with D_2O in the reverse micelles did not result in observable OD peaks in the 1D ^{2}H NMR spectrum (see Figure S3). We attribute this negative result to common challenges associated with ^{2}H NMR such as an approximately 7-fold decrease in sensitivity, lower resolution, and shorter T_1 times,[55] as documented for adaptation of ^{1}H to ^{2}H NMR in other studies.[56−58] Thus, we could not measure the exchange in an ^{2}H EXSY NMR experiment to confirm the isotope effect. Still, we believe that hydrogen atom tunneling is a good possibility given its demonstrated presence in similar low-temperature water systems.[54,59]

The barrier to hydrogen atom exchange as expressed by the calculated activation energies is more than 2.5 times higher for the 1β hydroxyl compared to the 1α position. Given our interpretation of a net orientation for intra-reverse-micellar glucose molecules from data in the high-temperature regime, this lower barrier for the 1α position may indicate stronger hydrogen bonding as the temperature drops, conceivably with water molecules trapped between the glucose and the reverse micelle interface.

We considered whether physical changes to our reverse micelle samples at low temperatures could be responsible for the low exchange barrier we measure. Other groups report water shedding from reverse micelles upon cooling to temperatures lower than the lowest temperatures we probed. Both Suzuki et al.[60] and Van Horn et al.[61] noted that AOT reverse micelles encapsulating only water—without added glucose—appear to shed water then form ice. Yet this behavior was only seen when cooled to temperatures below 252 K, the lowest temperature measured in this experiment. In low-temperature 1D ^{1}H NMR experiments, Klíčová et al. observed irreversible water shedding from reverse micelles leading to ice formation outside the micelles.[62] The persistence of water and glucose OH peaks in the EXSY NMR spectra over the entire temperature range we measured as well as the reproducibility of signals when temperatures were reached by either warming or cooling indicates that the aqueous interiors of the glucose-loaded reverse micelles remain liquid at all temperatures measured. It is not clear how water shedding or ice formation would lead to lower barriers to exchange that we observe.

Our reverse micelle size measurements display a modest increase in average diameter with decreasing temperature (Figure S4 and Table S3). If reverse micelles become larger at lower temperatures, we expect an increase rather than a decrease in the exchange rate as larger water pool should provide increased access to water molecules and reduced water network disruption. We might expect lower exchange rates if our samples were similarly sized to the results reported by Suzuki et al. and Van Horn et al., who both report far smaller reverse micelles than what we measure for our glucose loaded reverse micelles. Thus, the change in reverse micelle size that we observe does not provide a good explanation of the reduced barrier we observe in the low-temperature regime.

It is possible that lower temperatures could cause the intramicellar glucose molecules to experience a different environment from its location reverse micelles in the high-temperature regime. In previous work, we hypothesized that glucose resides near the AOT headgroups where it could shield the positive sodium atoms from the negatively charged AOT headgroups.[27,63] The increase in reverse micelle size with decreasing temperature could indicate glucose moving away from the interface, thus increasing reverse micelle volume. However, in this environment, we would again expect more facile hydrogen atom exchange with increased access to the

https://doi.org/10.1021/acs.jpcb.0c10681
J. Phys. Chem. B 2021, 125, 3364−3373

water pool. Likewise, a drop or rise in intramicellar pH should dramatically increase the exchange rate as the mechanism changes from concerted to charge transfer.[45]

The observation of two temperature regimes and subsequent proposition of hydrogen tunneling should give caution to the assumption that hydrogen atom exchange in confined biological spaces proceeds via a classical energy barrier. In fact, these data may indicate tunneling can occur at a relatively high temperature when water and glucose are in a nanoconfined space. The threshold temperature for the transition to tunneling may suggest that this phenomenon could occur more easily in biological system than previously thought. We have reduced the rate of exchange with the relatively simple act of reducing the space available to the glucose and water pool. This same method of nanoconfinement could be used to introduce energy barriers that allow for the study of previously unobserved high energy intermediates or transition state structures. The occurrence of hydrogen tunneling as a result of the low barrier hydrogen bond (LBHB) has been extensively studied,[64−66] and numerous other studies have begun to link hydrogen tunneling to biological systems, mostly in enzymatic catalysis.[67−70] Our results encourage this continued re-examination of such processes to search for an energy barrier previously presumed negligible.

CONCLUSION

Confinement of glucose and water within a w_0 = 10 reverse micelle retards the process of hydrogen atom exchange, making the unobservable exchange process in bulk solution measurable with ^{1}H EXSY NMR. For the first time, we report the value of this energy barrier to exchange. The unexpected departure from a single linear trend in the reported Arrhenius plot suggested differing mechanisms for hydrogen atom exchange at higher and lower temperatures.

Probing energy barriers present between water and other osmolytes extends beyond alternative carbohydrates like trehalose or fructose.[71,72] Because the preparation of reverse micelles results in a size-tunable, isolated droplet, this methodology can be easily extended to produce other simplified model environments. This work most directly benefits fields biotechnology or pharmacology, as they necessitate that researchers understand more complex chemical reactions at interfaces or in sequestered, nanosized pockets of enzymes or other biomolecules.

ASSOCIATED CONTENT

Supporting Information

The Supporting Information is available free of charge at https://pubs.acs.org/doi/10.1021/acs.jpcb.0c10681.

Example of methanol thermometer used to monitor sample temperature for EXSY NMR experiments (Figure S1); differential scanning calorimetry scan of glucose-loaded AOT reverse micelles over the temperature range for EXSY NMR experiments (Figure S2); ^{2}H NMR spectra of deuterium exchanged glucose in D_2O/AOT/isooctane reverse micelles (Figure S3); dynamic light scattering data as a function of temperature for glucose-loaded AOT reverse micelles (Figure S4); rate constants k_1 and k_2 for hydrogen exchange between water and glucose determined from EXSY NMR experiments and derived from eq 3 (Table S1); linear fit data for Arrhenius data shown in Figure 6 (Table S2); dynamic light scattering size distribution data as a function of temperature for glucose-loaded AOT reverse micelles (Table S3); temperature-dependent chemical shift of water peak data in NMR (Table S4) (PDF)

AUTHOR INFORMATION

Corresponding Author

Nancy E. Levinger − *Department of Chemistry, Colorado State University, Fort Collins, Colorado 80523-1872, United States;* orcid.org/0000-0001-9624-4867; Email: Nancy.Levinger@colostate.edu

Authors

Samantha L. Miller − *Department of Chemistry, Colorado State University, Fort Collins, Colorado 80523-1872, United States*

Benjamin P. Wiebenga-Sanford − *Department of Chemistry, Colorado State University, Fort Collins, Colorado 80523-1872, United States*

Christopher D. Rithner − *Department of Chemistry, Colorado State University, Fort Collins, Colorado 80523-1872, United States*

Complete contact information is available at: https://pubs.acs.org/10.1021/acs.jpcb.0c10681

Notes

The authors declare no competing financial interest.

ACKNOWLEDGMENTS

We gratefully acknowledge financial support from Colorado State University and NSF Grant 1956323. We thank Prof. Joseph DiVerdi for help with viscosity measurements and stimulating discussions. Additionally, we acknowledge Colorado State University as a land-grant institution that would not exist without the sale and exploitation of Indigenous territories in Colorado.

REFERENCES

(1) Gregory, J. *Particles in Water*, 1st ed.; Hoffmann, T., von Der Kammer, F., Eds.; Taylor & Francis Group: London, 2005.

(2) Eisenberg, D.; Kauzmann, W. *The Structure and Properties of Water*, 2nd ed.; Oxford University Press: New York, 2007.

(3) Steffel, L. R.; Cashman, T. J.; Reutershan, M. H.; Linton, B. R. Deuterium Exchange as an Indicator of Hydrogen Bond Donors and Acceptors. *J. Am. Chem. Soc.* **2007**, *129*, 12956−12957.

(4) Schneider, T. L.; Halloran, K. T.; Hillner, J. A.; Conry, R. R.; Linton, B. R. Application of H/D Exchange to Hydrogen Bonding in Small Molecules. *Chem. - Eur. J.* **2013**, *19*, 15101−15104.

(5) Kloiber, K.; Spitzer, R.; Grutsch, S.; Kreutz, C.; Tollinger, M. Longitudinal Exchange: An Alternative Strategy towards Quantification of Dynamics Parameters in ZZ Exchange Spectroscopy. *J. Biomol. NMR* **2011**, *51*, 123−129.

(6) Wolff, S. D.; Balaban, R. S. NMR Imaging of Labile Proton Exchange. *J. Magn. Reson.* **1990**, *86*, 164−169.

(7) Guivel-Scharen, V.; Sinnwell, T.; Wolff, S. D.; Balaban, R. S. Detection of Proton Chemical Exchange between Metabolites and Water in Biological Tissues. *J. Magn. Reson.* **1998**, *133*, 36−45.

(8) Agmon, N. The Grotthuss Mechanism. *Chem. Phys. Lett.* **1995**, *244*, 456−462.

(9) Brovchenko, I.; Oleinikova, A. Which Properties of a Spanning Network of Hydration Water Enable Biological Functions? *ChemPhysChem* **2008**, *9*, 2695−2702.

(10) Alba-Simionesco, C.; Coasne, B.; Dosseh, G.; Dudziak, G.; Gubbins, K. E.; Radhakrishnan, R.; Sliwinska-Bartkowiak, M. Effects

of Confinement on Freezing and Melting. *J. Phys.: Condens. Matter* **2006**, *18*, R15−R18.
(11) Takaiwa, D.; Hatano, I.; Koga, K.; Tanaka, H. Phase Diagram of Water in Carbon Nanotubes. *Proc. Natl. Acad. Sci. U. S. A.* **2008**, *105*, 39−43.
(12) Thostenson, E. T.; Ren, Z.; Chou, T. W. Advances in the Science and Technology of Carbon Nanotubes and Their Composites: A Review. *Compos. Sci. Technol.* **2001**, *61*, 1899−1912.
(13) Iijima, S. Helical Microtubules of Graphitic Carbon. *Nature* **1991**, *354*, 56−58.
(14) Wilson-Kubalek, E. M.; Brown, R. E.; Celia, H.; Milligan, R. A. Lipid Nanotubes as Substrates for Helical Crystallization of Macromolecules. *Proc. Natl. Acad. Sci. U. S. A.* **1998**, *95*, 8040−8045.
(15) Lee, J. K.; Banerjee, S.; Nam, H. G.; Zare, R. N. Acceleration of Reaction in Charged Microdroplets. *Q. Rev. Biophys.* **2015**, *48*, 437−444.
(16) Rosca, I. D.; Watari, F.; Uo, M. Microparticle Formation and Its Mechanism in Single and Double Emulsion Solvent Evaporation. *J. Controlled Release* **2004**, *99* (2), 271−280.
(17) Takei, T.; Mukasa, K.; Kofuji, M.; Fuji, M.; Watanabe, T.; Chikazawa, M.; Kanazawa, T. Changes in Density and Surface Tension of Water in Silica Pores. *Colloid Polym. Sci.* **2000**, *278*, 475−480.
(18) Chowdhury, S. R.; Schmuhl, R.; Keizer, K.; Ten Elshof, J. E.; Blank, D. H. A. Pore Size and Surface Chemistry Effects on the Transport of Hydrophobic and Hydrophilic Solvents through Mesoporous γ-Alumina and Silica MCM-48. *J. Membr. Sci.* **2003**, *225* (2), 177−186.
(19) Dodevski, I.; Nucci, N. V.; Valentine, K. G.; Sidhu, G. K.; O'Brien, E. S.; Pardi, A.; Wand, A. J. Optimized Reverse Micelle Surfactant System for High-Resolution. *J. Am. Chem. Soc.* **2014**, *136*, 3465−3474.
(20) Shi, Z.; Peterson, R. W.; Wand, A. J. New Reverse Micelle Surfactant Systems Optimized for High-Resolution NMR Spectroscopy of Encapsulated Proteins. *Langmuir* **2005**, *21*, 10632−10637.
(21) Radhakrishnan, R.; Gubbins, K. E.; Sliwinska-Bartkowiak, M. Global Phase Diagrams for Freezing in Porous Media. *J. Chem. Phys.* **2002**, *116*, 1147.
(22) Correa, N. M.; Silber, J. J.; Riter, R. E.; Levinger, N. E. Nonaqueous Polar Solvents in Reverse Micelle Systems. *Chem. Rev.* **2012**, *112*, 4569−4602.
(23) Piletic, I. R.; Moilanen, D. E.; Spry, D. B.; Levinger, N. E.; Fayer, M. D. Testing the Core/Shell Model of Nanoconfined Water in Reverse Micelles Using Linear and Nonlinear IR Spectroscopy. *J. Phys. Chem. A* **2006**, *110*, 4985−4999.
(24) Kinugasa, T.; Kondo, A.; Nishimura, S.; Miyauchi, Y.; Nishii, Y.; Watanabe, K.; Takeuchi, H. Estimation for Size of Reverse Micelles Formed by AOT and SDEHP Based on Viscosity Measurement. *Colloids Surf., A* **2002**, *204*, 193−199.
(25) Eastoe, J.; Robinson, B. H.; Steytler, D. C.; Thorn-Leeson, D. Structural Studies of Microemulsions Stabilised by Aerosol-OT. *Adv. Colloid Interface Sci.* **1991**, *36*, 1−31.
(26) Balakrishnan, S.; Javid, N.; Weingärtner, H.; Winter, R. Small-Angle X-Ray Scattering and near-Infrared Vibrational Spectroscopy of Water Confined in Aerosol-OT Reverse Micelles. *ChemPhysChem* **2008**, *9*, 2794−2801.
(27) Wiebenga-Sanford, B. P.; Washington, J. B.; Cosgrove, B.; Palomares, E. F.; Vasquez, D. A.; Rithner, C. D.; Levinger, N. E. Sweet Confinement: Glucose and Carbohydrate Osmolytes in Reverse Micelles. *J. Phys. Chem. B* **2018**, *122*, 9555−9566.
(28) Wiebenga-Sanford, B. P.; Diverdi, J.; Rithner, C. D.; Levinger, N. E. Nanoconfinement's Dramatic Impact on Proton Exchange between Glucose and Water. *J. Phys. Chem. Lett.* **2016**, *7*, 4597−4601.
(29) Silber, J. J.; Biasutti, A.; Abuin, E.; Lissi, E. Interactions of Small Molecules with Reverse Micelles. *Adv. Colloid Interface Sci.* **1999**, *82*, 189−252.
(30) Luisi, P. L.; Giomini, M.; Pileni, M. P.; Robinson, B. H. Reverse Micelles as Hosts for Proteins and Small Molecules. *Biochim. Biophys. Acta, Rev. Biomembr.* **1988**, *947*, 209−246.
(31) Vrignaud, S.; Benoit, J. P.; Saulnier, P. Strategies for the Nanoencapsulation of Hydrophilic Molecules in Polymer-Based Nanoparticles. *Biomaterials* **2011**, *32*, 8593−8604.
(32) Wiederschain, G. Y. Essentials of Glycobiology. *Biokhimiya* **2009**, *74*, 1056−1056.
(33) Taylor, M. E.; Drickamer, K.; Schnaar, R. L.; Etzler, M. E.; Varki, A. *Discovery and Classification of Glycan-Binding Proteins*, 2nd ed.; Varki, A., Etzler, M. E., Cummings, R. D., Esko, J. D., Eds.; The Consortium of Glycobiology: Cold Spring Harbor, 2015.
(34) Van Geet, A. L. Calibration of the Methanol and Glycol Nuclear Magnetic Resonance Thermometers with a Static Thermistor Probe. *Anal. Chem.* **1968**, *40*, 2227−2229.
(35) Bagno, A.; Rastrelli, F.; Scorrano, G. Detecting Intermolecular NOEs by Means of a Novel DPFGSE Pulse Sequence. Application to the Solvation of Carbohydrates in Binary Mixtures. *J. Magn. Reson.* **2004**, *167*, 31−35.
(36) Krishnamurthy, K. Hadamard Excitation Sculpting. *J. Magn. Reson.* **2001**, *153*, 144−150.
(37) Stott, K.; Keeler, J.; Van, Q. N.; Shaka, A. J. One-Dimensional NOE Experiments Using Pulsed Field Gradients. *J. Magn. Reson.* **1997**, *125*, 302−324.
(38) Mittermaier, A. ZZ-Exchange. In *Encyclopedia of Biophysics*; Roberts, G. C. K., Ed.; Springer: Berlin, 2013; pp 2796−2797.
(39) Webb, B.; Widek, T.; Neumayer, B.; Bruguier, C.; Scheicher, S.; Sprenger, H.; Grabherr, S.; Schwark, T.; Stollberger, R. Temperature Dependence of Viscosity, Relaxation Times (T1, T2) and Simulated Contrast for Potential Perfusates in Post-Mortem MR Angiography (PMMRA). *Int. J. Legal Med.* **2017**, *131*, 739−749.
(40) Tsukiashi, A.; Min, K. S.; Kitayama, H.; Terasawa, H.; Yoshinaga, S.; Takeda, M.; Lindoy, L. F.; Hayami, S. Application of Spin-Crossover Water Soluble Nanoparticles for Use as MRI Contrast Agents. *Sci. Rep.* **2018**, *8*, 14911.
(41) Lemmon, E. W.; McLinden, M. O.; Friend, D. G. *NIST Chemistry WebBook, NIST Standard Reference Database* https://webbook.nist.gov/chemistry/ (accessed 2020-10-31).
(42) Munshi, N.; De Tapas, K.; Maitra, A. Size Modulation of Polymeric Nanoparticles under Controlled Dynamics of Microemulsion Droplets. *J. Colloid Interface Sci.* **1997**, *190*, 387−391.
(43) De, T. K.; Maitra, A. Solution Behaviour of Aerosol OT in Non-Polar Solvents. *Adv. Colloid Interface Sci.* **1995**, *59*, 95−193.
(44) Delgado, M.; Lázaro, A.; Biedenbach, M.; Gamisch, S.; Gschwander, S.; Höhlein, S.; König-Haagen, A.; Brüggemann, D. Intercomparative Tests on Viscosity Measurements of Phase Change Materials. *Thermochim. Acta* **2018**, *668*, 159−168.
(45) Hills, B. P. Multinuclear NMR Studies of Water in Solutions of Simple Carbohydrates. *Mol. Phys.* **1991**, *72*, 1099−1121.
(46) Harvey, J. M.; Symons, M. C. R.; Naftalin, R. J. Proton Magnetic Resonance Study of the Hydration of Glucose. *Nature* **1976**, *261*, 435−436.
(47) Tait, M. J.; Suggett, A.; Franks, F.; Ablett, S.; Quickenden, P. A. Hydration of Monosaccharides: A Study by Dielectric and Nuclear Magnetic Relaxation. *J. Solution Chem.* **1972**, *1* (2), 131−151.
(48) Laage, D.; Hynes, J. T. A Molecular Jump Mechanism of Water Reorientation. *Science* **2006**, *311*, 32−835.
(49) Zhang, Q.; Wu, T. M.; Chen, C.; Mukamel, S.; Zhuang, W. Molecular Mechanism of Water Reorientational Slowing down in Concentrated Ionic Solutions. *Proc. Natl. Acad. Sci. U. S. A.* **2017**, *114*, 10023−10028.
(50) Meng, X.; Guo, J.; Peng, J.; Chen, J.; Wang, Z.; Shi, J. R.; Li, X. Z.; Wang, E. G.; Jiang, Y. Direct Visualization of Concerted Proton Tunnelling in a Water Nanocluster. *Nat. Phys.* **2015**, *113*, 235−239.
(51) Li, X. Z.; Probert, M. I. J.; Alavi, A.; Michaelides, A. Quantum Nature of the Proton in Water-Hydroxyl Overlayers on Metal Surfaces. *Phys. Rev. Lett.* **2010**, *104*, 066102.
(52) Laage, D.; Stirnemann, G.; Sterpone, F.; Rey, R.; Hynes, J. T. Reorientation and Allied Dynamics in Water and Aqueous Solutions. *Annu. Rev. Phys. Chem.* **2011**, *62*, 395−416.
(53) Ceriotti, M.; Fang, W.; Kusalik, P. G.; McKenzie, R. H.; Michaelides, A.; Morales, M. A.; Markland, T. E. Nuclear Quantum

https://doi.org/10.1021/acs.jpcb.0c10681
J. Phys. Chem. B 2021, 125, 3364−3373

Effects in Water and Aqueous Systems: Experiment, Theory, and Current Challenges. *Chem. Rev.* **2016**, *116*, 7529−7550.
(54) Drechsel-Grau, C.; Marx, D. Collective Proton Transfer in Ordinary Ice: Local Environments, Temperature Dependence and Deuteration Effects. *Phys. Chem. Chem. Phys.* **2017**, *19*, 2623−2635.
(55) Sattler, M.; Fesik, S. W. Use of Deuterium Labeling in NMR: Overcoming a Sizeable Problem. *Structure* **1996**, *4*, 1245−1249.
(56) Marshall, A. G. Calculation of NMR Relaxation Times for Quadrupolar Nuclei in the Presence of Chemical Exchange. *J. Chem. Phys.* **1970**, *52*, 2527−2534.
(57) Ludwig, R. NMR Relaxation Studies in Water-Alcohol Mixtures: The Water-Rich Region. *Chem. Phys.* **1995**, *195*, 329−337.
(58) Schönhoff, M. NMR Methods for Studies of Organic Adsorption Layers. In *Studies in Interface Science*; Max Planck Institute: Potsdam, 2001.
(59) Drechsel-Grau, C.; Marx, D. Quantum Simulation of Collective Proton Tunneling in Hexagonal Ice Crystals. *Phys. Rev. Lett.* **2014**, *112*, 148300−148302.
(60) Suzuki, A.; Yui, H. Crystallization of Confined Water Pools with Radii Greater than 1 nm in AOT Reverse Micelles. *Langmuir* **2014**, *30*, 7274−7282.
(61) Van Horn, W. D.; Ogilvie, M. E.; Flynn, P. F. Reverse Micelle Encapsulation as a Model for Intracellular Crowding. *J. Am. Chem. Soc.* **2009**, *131*, 8030−8039.
(62) Klíčová, L.; Muchová, E.; Šebej, P.; Slavíček, P.; Klán, P. Nature of CTAB/Water/Chloroform Reverse Micelles at Above- and Subzero Temperatures Studied by NMR and Molecular Dynamics Simulations. *Langmuir* **2015**, *31*, 8284−8293.
(63) Kamboj, R.; Bharmoria, P.; Chauhan, V.; Singh, G.; Kumar, A.; Singh, S.; Kang, T. S. Effect of Cationic Head Group on Micellization Behavior of New Amide-Functionalized Surface Active Ionic Liquids. *Phys. Chem. Chem. Phys.* **2014**, *16*, 26040−26050.
(64) Tuckerman, M. E.; Marx, D.; Klein, M. L.; Parrinello, M. On the Quantum Nature of the Shared Proton in Hydrogen Bonds. *Science* **1997**, *275*, 817−820.
(65) Perrin, C. L. Are Short, Low-Barrier Hydrogen Bonds Unusually Strong? *Acc. Chem. Res.* **2010**, *43*, 1550−1557.
(66) Shokri, A.; Wang, Y.; O'Doherty, G. A.; Wang Bin, X.; Kass, S. R. Hydrogen-Bond Networks: Strengths of Different Types of Hydrogen Bonds and an Alternative to the Low Barrier Hydrogen-Bond Proposal. *J. Am. Chem. Soc.* **2013**, *135*, 17919−17924.
(67) Ishikita, H.; Saito, K. Proton Transfer Reactions and Hydrogen-Bond Networks in Protein Environments. *J. R. Soc. Interface* **2014**, *11*, 1742−1753.
(68) Cleland, W. W.; Kreevoy, M. M. Low-Barrier Hydrogen Bonds and Enzymic Catalysis. *Science* **1994**, *44*, 1−17.
(69) Schiøtt, B.; Iversen, B. B.; Madsen, G. K. H.; Larsen, F. K.; Bruice, T. C. On the Electronic Nature of Low-Barrier Hydrogen Bonds in Enzymatic Reactions. *Proc. Natl. Acad. Sci. U. S. A.* **1998**, *95*, 12799−12802.
(70) Dai, S.; Funk, L. M.; von Pappenheim, F. R.; Sautner, V.; Paulikat, M.; Schröder, B.; Uranga, J.; Mata, R. A.; Tittmann, K. Low-Barrier Hydrogen Bonds in Enzyme Cooperativity. *Nature* **2019**, *573*, 609−613.
(71) Wand, A. J. Bringing Disorder and Dynamics in Protein Allostery into Focus. *Proc. Natl. Acad. Sci. U. S. A.* **2017**, *114*, 4278−4280.
(72) Nucci, N. V.; Pometun, M. S.; Wand, A. J. Site-Resolved Measurement of Water-Protein Interactions by Solution NMR. *Nat. Struct. Mol. Biol.* **2011**, *18*, 245−249.

https://doi.org/10.1021/acs.jpcb.0c10681
J. Phys. Chem. B 2021, 125, 3364−3373